# Numerical Prediction on the Crashworthiness of Circular and Square Thin-Walled Tubes with Polymeric Auxetic Foam Core

S. Mohsenizadeh, Z. Ahmad, and A. Alias

*(Submitted September 24, 2019; in revised form April 14, 2020; published online May 22, 2020)*

**This present research numerically investigates the energy absorption capability of auxetic foam-filled tubes when loaded statically. Accordingly, numerical simulations were performed to quantify the influence of tubes' parameters such as wall thickness, diameter and width on the energy absorption responses and deformation modes of auxetic foam-filled circular and square tubes using validated FE models. The results reveal that the progressive collapse and deformation mode of auxetic foam-filled circular tube are pronouncedly affected by varying the tube width, so that the number of lobes created decreases as the tube width increases. Moreover, it was found that the absorbed energy by auxetic foam-filled square tube shows more dependence on the tube wall thickness variations than on the tube width. Nonetheless, increasing the width of filled tube makes the structure heavier without considerably affecting the absorbed energy, which is undesirable in design of energy absorbing structures. The primary outcome of this research is a design guideline for the use of auxetic foam as a core for an energy absorber device where impact loading is expected.**

## 1. Introduction

Increased interest in vehicle safety and crashworthiness has led to considerable investigations on crush response, energy absorption capability, and progressive collapse mode of energy absorbing devices from experimental, analytical and numerical points of view (Ref 1-6). Thin-walled tubular structures as effective energy absorbing devices have been impressively considered in structural impact applications for mitigating adverse effect of impact with controllable deformation. Therefore, thin-walled tubes have been extensively utilized in automobile industry since they are excellent at dissipating kinetic energy by progressive plastic deformation when subjected to different loading conditions (Ref 7, 8). On the other hand, the combination of thin-walled structures with cellular materials like metallic and non-metallic foams, honeycombs structures (aluminum honeycomb) and tube filler was another reason for the great interest in the use of thin-walled structures as energy absorbing devises (Ref 9-15). Therefore, a considerable amount of literature has been published which investi-

gate the deformation behavior and energy absorption characteristic of thin-walled structures in different cross sections and materials (Ref 16). For instance, crushing behavior and deformation modes of circular, rectangular, square, triangular, pyramidal, hexagonal and conical tubes under compressive axial loading were studied. Results of a study carried out by Nia and Parsapour (Ref 17) indicated that the cylindrical and triangular tubes exhibit the highest and lowest energy absorption capacity under compressive axial loading, respectively. Recently, Liu et al. (Ref 18) investigated experimentally and numerically the crush response of multi-corner tubes (star-shaped) under dynamic loading condition. Fan et al. (Ref 19) carried out a series of experimental tests in which they investigated the crush characteristic and deformation mechanism of equilateral triangular cross section tubes when loaded statically.

Although, for many decades, several attempts have been made to design thin-walled tubes with minimum mass but higher energy absorption capacity, foam-filled thin-walled tubes have gained increased attention in the literature. This is due to great performance of foam-filled tubes when loaded axially or obliquely compared with empty tubes. Hence, much effort was made to predict the deformation profile, crush response and energy absorption behavior of foam-filled tubes under quasi-static and dynamic loading (Ref 13, 20-23). In this regard, energy absorption capacity of filled tubes was investigated when lightweight materials such as polyurethane foams, wood (Ref 24), cork (Ref 25), metal foams (Ref 26), carbon nanopolyurethane foam (Ref 27) and polystyrene foams (Ref 9, 28) were introduced as the cores. However, polymeric and aluminum foams have attained increased attention as the cores of thin-walled tubes due to their great potential for promoting strain energy dissipation of structures and stabilizing the crush responses of tubes.

In 1988, Reddy and Wall (Ref 29) investigated experimentally and numerically the effect of low density polymeric foam

**S. Mohsenizadeh, Z. Ahmad,** and **A. Alias,** School of Mechanical Engineering, Faculty of Engineering, Universiti Teknologi Malaysia, 81310 Johor Bahru, Malaysia. Contact e-mail: azaini@utm.my.

on the crush response and energy absorption capacity of circular tubes when loaded dynamically and statically. The authors asserted that a considerable enhancement in the energy absorption capacity of circular tube can be attained by filling it with polyurethane foam. Experimental and numerical study on circular aluminum alloy 6060-T4 filled with Hydro Aluminum AS foam under axial and oblique quasi-static loading was conducted by Børvik et al. (Ref 30). Results indicate that the presence of foam core has insignificant effect on the initial peak load, but the mean crushing force (MCF) is noticeably enhanced by using the foam core. Recently, the potential utilization of polyurethane foam as a core of flax/epoxy circular tube when subjected to axial loading was investigated experimentally by Yan et al. (Ref 31). They found that the use of foam filler enhanced remarkably the specific energy absorption response and total absorbed energy of filled tubes compared with the empty one. In general, interaction effects between the tube walls and the foam core and the compression of foam core itself are the main mechanisms which lead to the enhancements (compared to empty tubes). Indeed, interaction effect leads to greater energy absorption (EA) of tube owing to altered deformation profile and enhances the energy absorption of foam core due to multiaxial compression (Ref 32). Furthermore, the increased number of lobes created and the controlled deformation profile of the tube walls by introducing the foam core is referred to as an interaction effect (Ref 33). Numerous researchers have contributed to this topic (Ref 10, 26, 28). For instance, Hanssen et al. (Ref 26) investigated axial deformation behavior of foam-filled circular tube under both dynamics and quasi-static axial loadings. From the presented results, a remarkable shift from the diamond profile to concertina profile occurred by introducing the foam core. This change of profile accounted for the interaction effect between the foam core and circular tube (Ref 26). In another investigation into the crushing response of foam-filled square tubes, Santosa et al. (Ref 3) reported that, for the foam-filled square tubes, more lobes were created and each lobe showed a larger curvature when compared with the lobes of empty tube which is due to the interaction effect between foam core and tube walls.

Most foam materials inserted in the tubes have a level of capacity to absorb energy. One of the most common specifications is to have positive Poisson's ratio or zero Poisson's ratio. In recent decade, a special interest has been shown in invention of foams with negative Poisson's ratio (NPR). Such foam materials that exhibit NPR are termed auxetic (Ref 34, 35). Auxetic materials show an opposite behavior in which lateral expansion occurs during the longitudinal stretch and vice versa (Ref 36). Auxetic foam material has gained popularity as a filler of thin-walled tube due to its enhanced mechanic properties compared with conventional foam. A remarkable amount of literature has been published on enhanced mechanical properties of auxetic foam such as superior energy dissipation, indentation resistance and higher fracture toughness (Ref 37-39). Regarding crush behavior, the research information on the using auxetic foam inside the thin-walled structure as an absorber is still limited, despite their potential to be an effective energy absorber. The result obtained by Hou et al. (Ref 40), who carried out a series of finite element (FE) simulations to investigate auxeticity effect of metallic foam on structural crashworthiness, indicated that energy absorption capability of metallic auxetic foam-filled tube is higher than that of metallic conventional foam-filled tube. The results obtained by Mohsenizadeh et al. (Ref 41, 42) who compared crashworthiness performance of conventional and auxetic foam-filled square tubes under quasi-static axial loading, also reported that energy absorption characteristic of the tube is significantly increased by introducing the auxetic foam as a core.

Due to the deficiency of research for auxetic foam application in crashworthiness, this study aims to evaluate the influence of geometrical parameter such as wall thickness, tube diameter and tube width on the energy absorption capacity of auxetic foam-filled tubes which enable efficient design of auxetic foam-filled tubes (square and circular cross sections) as energy absorbing devices. Practically, information obtained from this study can be employed to develop design guidelines for the use of auxetic foam-filled tubes as efficient energy absorbers, like vehicle protective structures. This will lead to an increase in the level of safety to the occupants of vehicles.

## 2. Materials and Experimental Work

### 2.1 Materials Properties

In this study, extruded circular and square tubes made of an aluminum alloy were used in the experimental tests. Based on the limitation of the foam core size and availability, square and circular thin-walled tubes were fabricated. The geometrical configurations and dimensions of the tubes are given in Fig. 1.

Mechanical properties of tube specimens were extracted through a standard tensile test in accordance with ASTM E8M (Ref 43). Tensile test was conducted using an INSTRON universal testing machine (UTM) which is equipped with the load-cell capacity of 5 kN. The test was performed at a constant loading rate of 1 mm/min. For accuracy and repeatability of measurement, five samples cut from the walls of the extruded tubes and parallel to the direction of extrusion were tested. The typical engineering stress–strain curves and mechanical properties of tube specimens including yield stress ($\sigma_y$), Young's modulus ($E$), fracture strain ($\varepsilon_f$) and ultimate tensile stress ($\sigma_u$) which were directly obtained from the results of the tensile test are presented in Fig. 2.

Conventional polymeric closed-cell foam with the density of 45 kg/m$^3$ was utilized to fabricate auxetic foam. Auxeticity process was carried out as described by Mohsenizadeh et al.
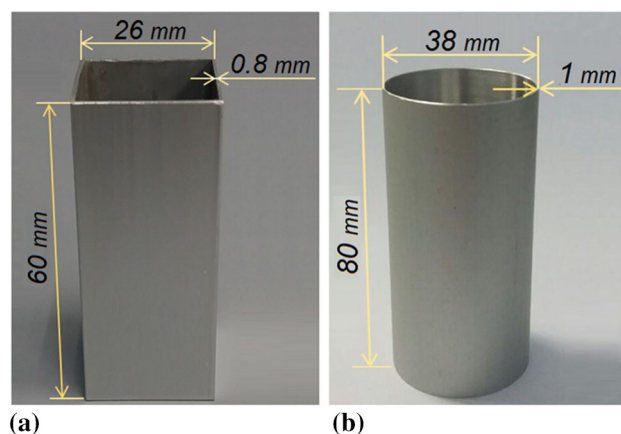


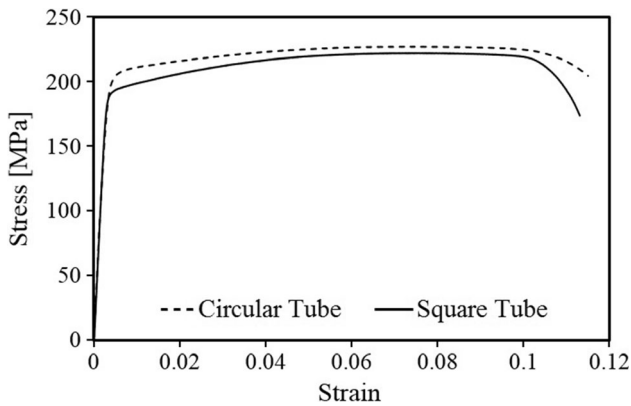**Fig. 1** Geometrical configuration and tube dimensions for (a) square and (b) circular tubes

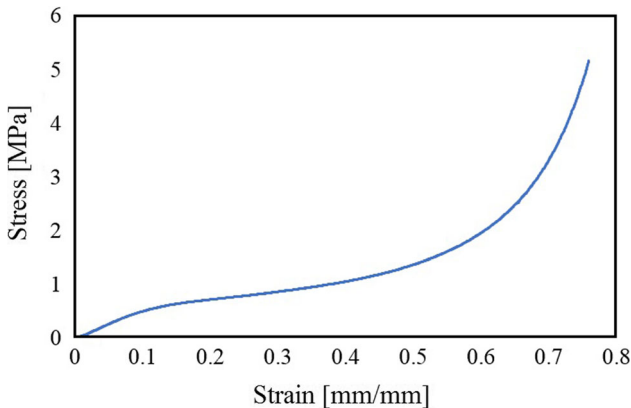**Fig. 2** Stress–strain curves of aluminum tubes



**Fig. 3** Stress–strain curve of auxetic foam

(Ref 44). Mechanical properties of fabricated auxetic foam were explored using uniaxial compression tests in accordance with ASTM D3574-95 (Ref 45). Test sample was compressed between two parallel jaws of UTM at a constant crosshead speed of 1 mm/min. In reducing experimental errors and enable repeatability, five samples were tested, and the average values were considered to define the mechanical behavior of fabricated foam. Stress–strain curve of fabricated auxetic foam under uniaxial compression test is illustrated in Fig. 3.

Furthermore, tensile stress of fabricated auxetic foam, together with the corresponding tensile strain as the required input parameters of foam's material model in FE simulation, was obtained using standard tensile test in accordance with ASTM D3574-95 (Ref 45). Tensile test sample and test set-up are shown in Fig. 4(a) and (b), respectively. A special fixture was designed to adapt the specimen for the test condition as illustrated in Fig. 4(b). This fixture consists of top and bottom parts which are fixed in the upper and lower grips of the testing machine, respectively, while the tensile load was applied by moving up the top part while the bottom part is fixed. To obtain an unambiguous state of stress in the reduced section, the test sample was pulled directly in line with the load cell such that it was free of any bending moment. The test was conducted at a speed of 1 mm/min. For minimizing experimental errors and enable repeatability, five tensile test samples of each foam were tested. However, only three test results for auxetic foam are presented in Fig. 5.

## 2.2 Specimens and Experimental Test

The foam cores (fabricated auxetic foam) were cut in a rectangular cuboid and circular cylinder shapes using a foam cutter. Aluminum empty tubes (square and circular sections) were then tightly filled with these resized foams as tube specimens.

A series of quasi-static compression tests was carried out on the tube specimens with the aim of verification the validity of finite element simulations. Quasi-static compression test was performed using an INSTRON universal testing machine which is equipped with a load-cell of capacity 50 kN. The load was applied at a rate of 3 mm/min to establish quasi-static condition and deformation of structure statically. All quasi-static test specimens were crushed up to 60% of their original length. For each case, load versus displacement curve was obtained. The deformation modes and load–displacement curves of the tube specimens under quasi-static axial loading are presented in the preceding section.

## 3. Finite Element Analysis

The development of the FE model for auxetic foam-filled tubes (square and circular cross sections) under quasi-static axial loading is described in this section. The explicit nonlinear commercial finite element code LS-DYNA was employed for all FE modeling. The FE models are validated using experimental results by comparing the deformation modes and load–displacement curves. Indeed, the validation process is indispensable to ensure accuracy and validity of the FE model. The validated FE models are then employed to subsequently carry out a series of parametric studies. In particular, a parametric study is used to evaluate the influence of geometrical parameters on the energy absorption performance and deformation mode of foam-filled tubes under axial loading condition. Figure 6 indicates the flowchart of the FE model developed in this study. Detailed description and key aspects of the FE model namely material model, geometry, FE mesh, boundary conditions, interaction, loading, control option and stability are thoroughly elaborated in the following subsections.

### 3.1 FE Discretization

The FE model of a foam-filled tube comprises of four parts namely rigid stationary plate, rigid movable mass, foam core and deformable square tube, as shown in Fig. 7. The stationary plate and movable mass were modeled as rigid parts for enhancement of computational efficiency. The tubes were modeled using quadrilateral Belytschko–Lin–Tsay shell element with five integration points through the thickness and one integration point in the elemental plane. It is noteworthy that greater computational efficiency is obtained using Belytschko–Lin–Tsay shell element formulation than other element formulation (Ref 46). The foam core was meshed using eight-node solid element with the reduced integration technique in combination with hourglass control. Stiffness-based hourglass control is adopted to avoid spurious zero energy deformation modes, and reduced integration is utilized to avoid volumetric locking (Ref 46).
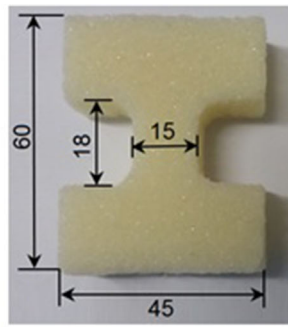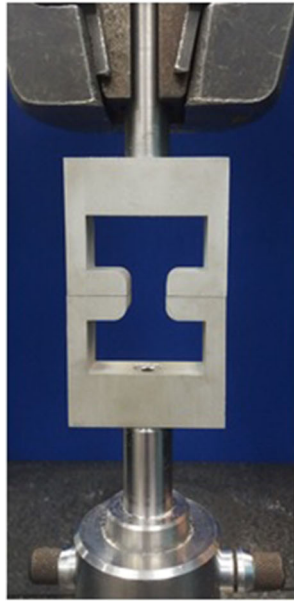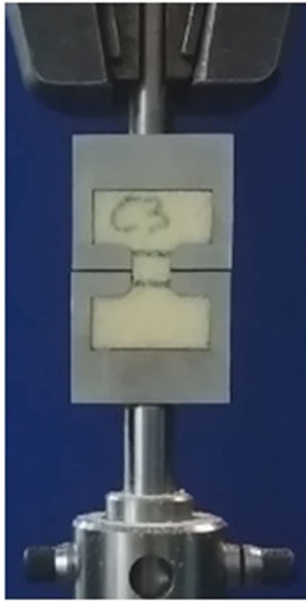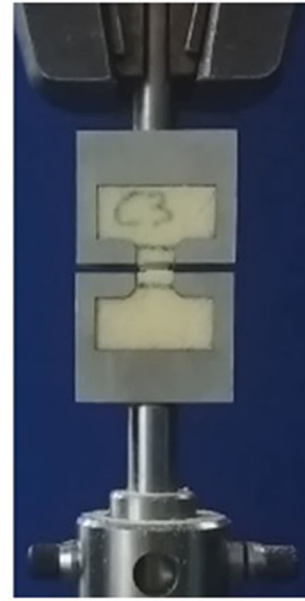
**Fig. 4** (a) Tensile test sample, (b) test set-up, (c) loading process and (d) end of test
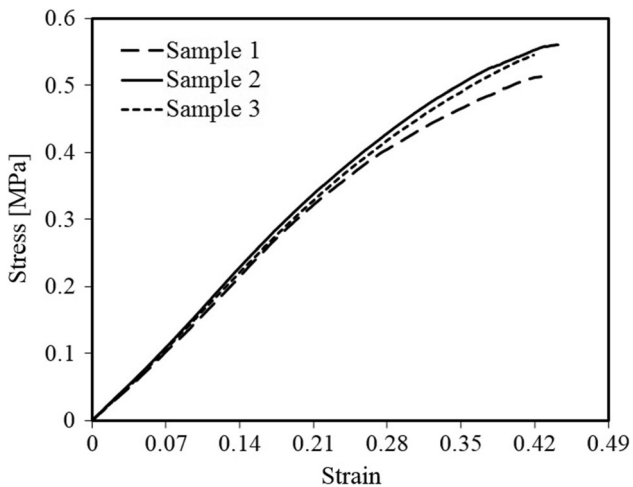


**Fig. 5** Tensile stress–strain curve for fabricated auxetic foam

### 3.2 Mesh Refinement

A mesh convergence study was performed with the aim of obtaining optimum element size for aluminum tube and foam core. Mesh refinement process is accomplished by reducing the element size (ES) since the accuracy of numerical model is directly affected by varying mesh sizes. Hence, for aluminum empty tube, different element sizes (5, 4, 3, 2.5, 2, 1.5, 1 and 0.5 mm) were used (Fig. 8) and the convergence of initial peak load and energy absorption versus element size were achieved as shown in Fig. 9. The results indicate that element size of 1 mm for the aluminum tube is found to be sufficient and suitable in producing accurate and reliable results. Thereby, further reduction of element size only increases the computational time with negligible alteration of initial peak load and absorbed energy (less than 2%). In addition, to find optimal element size for foam core, mesh refinement process was conducted anew for a foam-filled tube when the element size for tube was kept constant (1 mm) while it was varied from 6 to 2 mm for foam core, as shown in Fig. 10. From Fig. 11, it appears that the convergence of initial peak load and energy absorption versus *ES* was obtained when foam element size is ≤ 2.5 mm. Above all, in this simulation, element sizes of 1 and 2.5 mm were chosen for aluminum tube and foam core, respectively. Figure 12 shows the FE model with the optimum mesh size.

### 3.3 Material Model

MAT_24 (MAT_PIECEWISE_LINEAR_PLASTICITY) material model is adopted to model the aluminum tubes. The

engineering stress–strain data point is converted to true stress–strain data point and incorporated into the material model to represent plastic hardening behavior. The plastic hardening behavior of the tubes was calculated using the well-known fundamental equations in classical mechanics as follows (Ref 47).

$$\sigma_{True} = \sigma_{Eng}\left(1 + \varepsilon_{Eng}\right) \qquad (Eq\ 1)$$

$$\varepsilon_{Plastic} = \ln\left(1 + \varepsilon_{Eng}\right) - \frac{\sigma_{true}}{E} \qquad (Eq\ 2)$$

In the above equations, $\sigma_{True}$ and $\sigma_{Eng}$ are the true and engineering stresses, respectively. Similarly, $\varepsilon_{Plastic}$ and $\varepsilon_{Eng}$ are the true and engineering plastic strains. As shown in Eq 1, true stress is expressed in terms of engineering stress considering both consistency of volume and a homogeneous distribution of strain along the gage length of the tensile test sample (Ref 47). Furthermore, the material properties of tubes such as Young's modulus and yield stress, obtained via standard tensile test, were used as the required input parameters into the material model (Table 1). The true stress ($\varepsilon_{True}$) and plastic strain ($\varepsilon_{Plastic}$) data points of square and circular tubes are given in Tables 2 and 3, respectively. Due to the strain rate insensitivity of the aluminum alloy, the strain rate effect was ignored in this model (Ref 40, 48).

MAT_063 (MAT_CRUSHABLE_FOAM) material model is defined for the auxetic foam. This material model is suitable for modeling the crushable foam with high efficiency and performance in terms of computational time, as reported in the literature (Ref 49). Table 4 shows the required input parameters for MAT_063. The compressive stress–strain relation and mechanical properties of auxetic foam obtained from the experimental tests which were included in the material model are presented in Fig. 3(b) and Table 5, respectively. In the FE simulation of foam material, Young's modulus ($E$) obtained from compressive stress–strain curve must be considered for foam material model as shown in Table 4. It is important to have a nonzero value for the tensile stress cutoff in order to prevent deterioration of the material under small tensile loads (Ref 50).

For modeling the rigid bodies (stationary plate and rigid movable mass), MAT_20 (MAT_RIGID) material model is assigned.

### 3.4 Boundary Conditions, Loading and Interaction

The stationary plate was fully constrained in all degrees of freedom, and the rigid movable mass was constrained to only translate vertically along the z axis as shown in Fig. 7. The motion of the rigid movable mass was defined using a prescribed motion in load curve. For this quasi-static simulation, prescribed velocity boundary condition is used for the rigid movable mass to simulate the displacement- controlled experiment. In particular, a ramp velocity–time history was prescribed for the rigid movable mass over a crushing duration as the velocity was initially ramped up then followed by a constant value of 0.5 m/s throughout the total loading duration in order to achieve an accurate and efficient quasi-static analysis. Generally, inertia effect is duly minimized by ramping the velocity in the static loading. A similar approach for FE model under quasi-static loading has been utilized previously in established studies (Ref 52, 53).

The interaction effect between the tube and foam was modeled using contact algorithm. In this simulation, three different contact algorithms were defined in this FE model. An automatic node to surface contact was selected for the contact interfaces of the tube and rigid plates. Also, self-contact algorithm was adopted for the tube in order to avoid interpenetration of the tube folding during the crushing process using "automatic_single_surface". To account for the contact
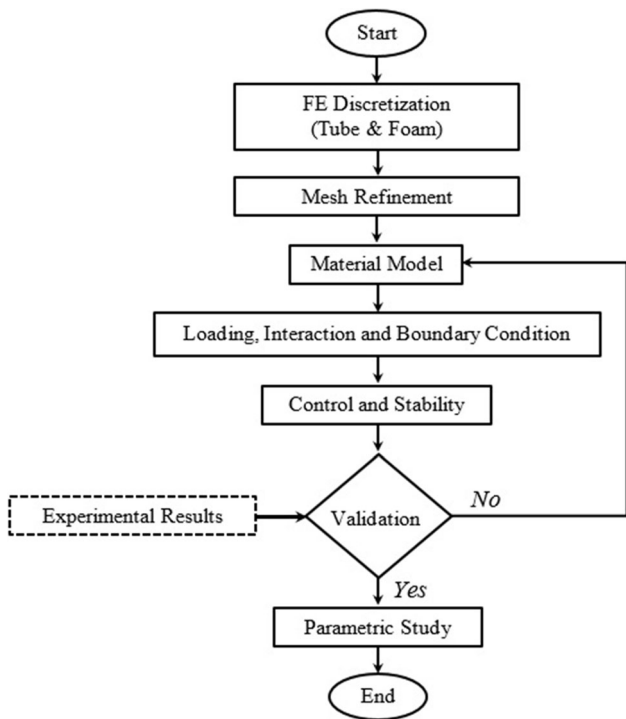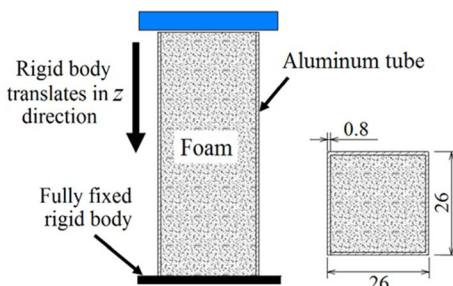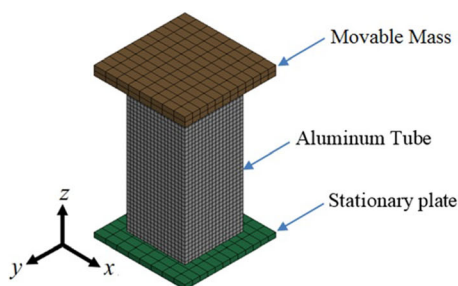


**Fig. 6** FE modeling flowchart



**Fig. 7** Geometrical model, tube dimension, loading and boundary condition arrangement of FE model for foam-filled tube

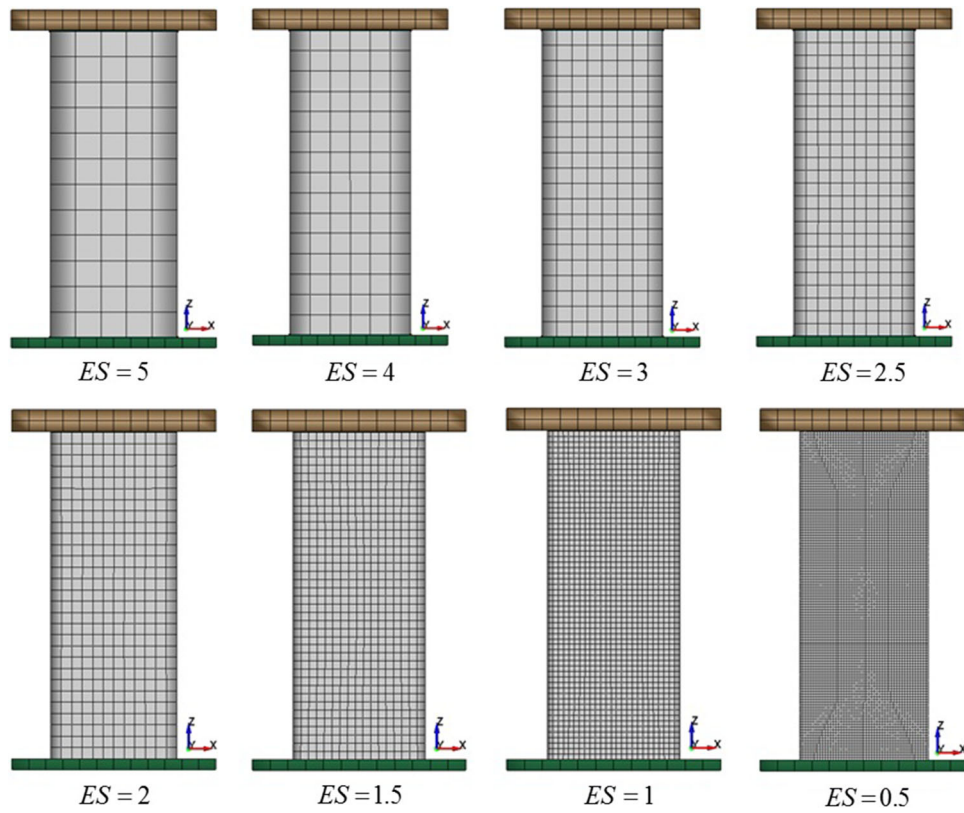**Fig. 8** Mesh refinement study for aluminum empty tube when the element size varies from 5 to 0.5 mm
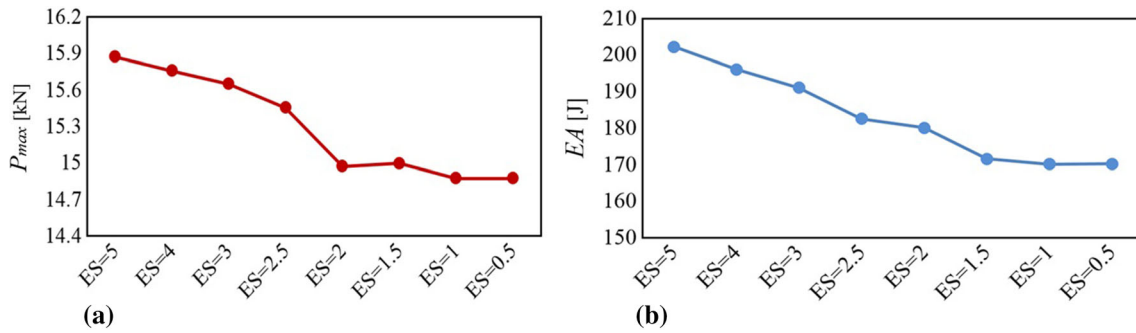


**Fig. 9** Verification of mesh element size for aluminum empty tube based on convergence of (a) initial peck load vs. element size and (b) energy absorption vs. element size
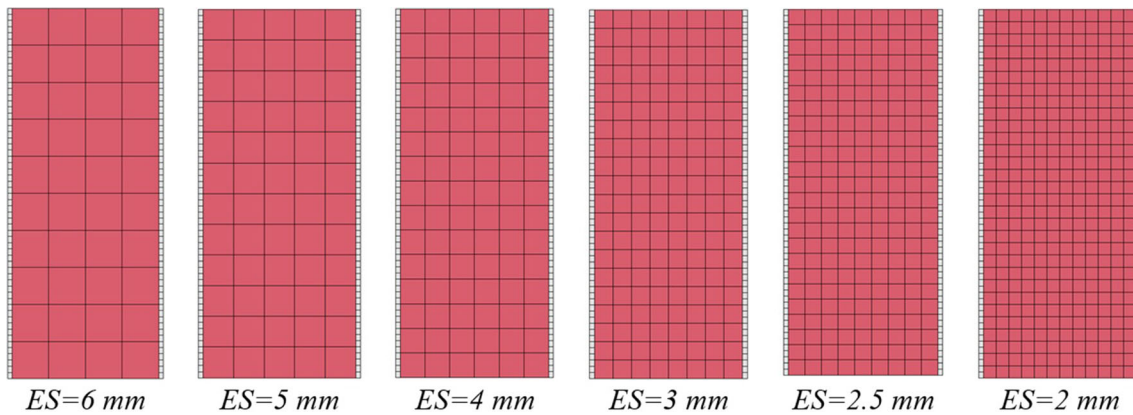


**Fig. 10** Mesh refinement study for foam-filled tube when the element size of foam core varies from 6 to 2 mm
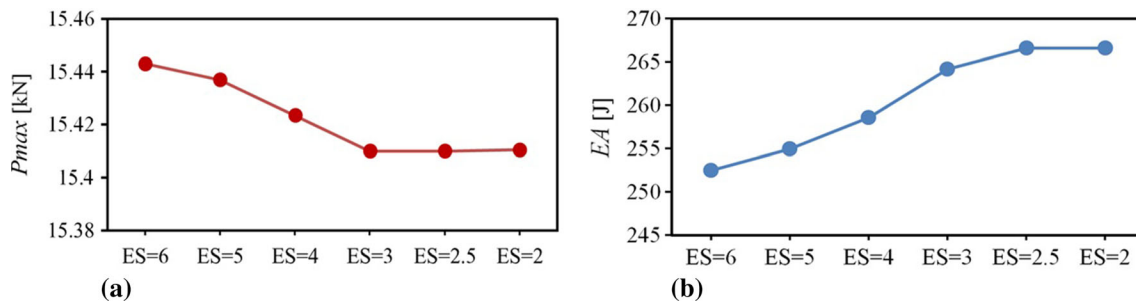
**Fig. 11** Verification of mesh element size for foam-filled tube based on convergence of (a) initial peck load vs. element size and (b) energy absorption vs. element size
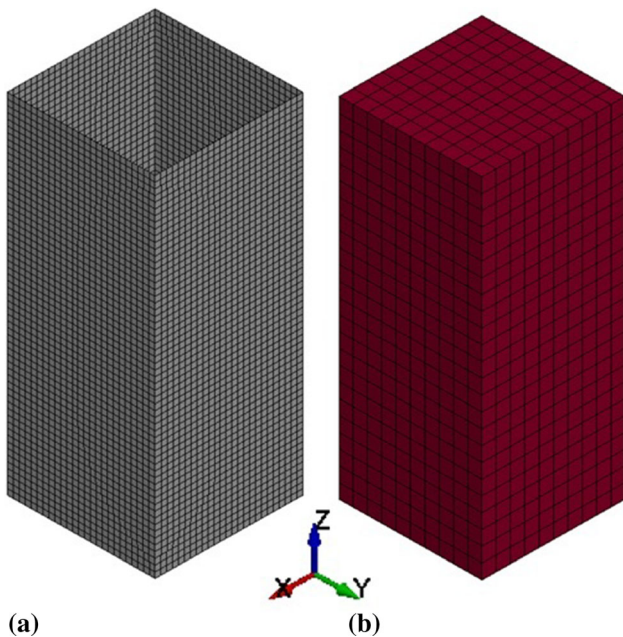


**Fig. 12** Finalized meshed model; (a) tube ES = 1 mm (b) foam ES = 2.5 mm

**Table 1  Mechanical properties of aluminum tubes**

| Mechanical properties | Symbol | Square tube | Circular tube |
|---|---|---|---|
| Young's modulus | $E$ (GPa) | 69.2 | 68.3 |
| Yield stress | $\sigma_y$ (MPa) | 192 | 208 |
| Ultimate tensile stress | $\sigma_u$ (MPa) | 221 | 226 |
| Poisson's ratio | $\upsilon$ | 0.33 | 0.33 |
| Density | $\rho$ (kg/m$^3$) | 2700 | 2700 |

interface between the foam filler, rigid parts and tube wall, an automatic surface to surface contact was simulated with dynamic and static frictional coefficients of 0.2 and 0.3, respectively (Ref 54).

### 3.5 Control and Stability

Mesh tangling is a problematic issue in modeling of foam materials owing to the highly compressible nature of such types of materials, which routinely undergoes 70-80% compression. In this regard, interior contact was employed with default activation thickness factor $F_a = 0.1$ to avoid mesh tangling in

high compression area (Ref 49, 55, 56). When the crushing of the element reaches $F_a$ times the initial thickness, the contact algorithm begins to act (Ref 55). However, the interior contact carries a computational penalty. The deformed profile of FE model under quasi-static axial loading is illustrated in Fig. 13. Similarly, the FE model for circular tube follows the same trend as the square tube does, and it is not shown here for the sake of brevity.

## 4.  Validation of FE Models and Parametric Study

Figure 14(a) and 15(a) compares the experimental and the numerical deformation profile for auxetic foam-filled circular tube (AFFCT) and auxetic foam-filled square tube (AFFST), respectively. The deformation profiles predicted by the FE models agree well with the experimental results. Hence, the FE models could simulate the physical responses of tubes under quasi-static axial loading. Another interest in validating the numerical model is the load–displacement curve and absorbed energy response simulated by the FE models. The load–displacement curves and the absorbed energy responses versus displacement predicted by the FE models as compared with those from the experimental results are shown in Fig. 14(b), (c) and 15(b), (c). It is evident that a good correlation between the numerical and experimental results has been obtained. Therefore, the validated FE models can be utilized to conduct a series of parametric study on the axial crushing of AFFCT and AFFST for various geometries under quasi-static axial loading. Tube effective parameters for square and circular tubes are given in Fig. 1.

It is noteworthy that the FE results are usually slightly higher than the experimental results. The inevitable discrepancy between these two results is due to the ideality of FE model configuration unlike the experimental specimens in which possible imperfection in the tube and foam materials caused by manufacturing process are involved. Moreover, the contacting surface between foam and tube in the simulation was modeled perfectly without any gap between the foam and tube wall which is rarely possible in the experimental specimen.

### 4.1 Influence of Wall Thickness on the Collapse Profile of AFFCT

From crashworthiness perspective, progressive buckling of cylindrical tubes in axisymmetric mode is more advantageous in energy absorbing systems because it dissipates greater strain energy than non-axisymmetric mode. In order to gain a far

**Table 2  True stress vs. plastic strain for square aluminum alloy in the FE model**

| $\varepsilon_{Plastic}$ | 0.0 | 0.013 | 0.026 | 0.039 | 0.051 | 0.065 | 0.078 | 0.091 |
|---|---|---|---|---|---|---|---|---|
| $\sigma_{True}$ (N/mm$^3$) | 192 | 206 | 217 | 227 | 233 | 237 | 240 | 241 |

**Table 3  True stress vs. plastic strain for circular aluminum alloy in the FE model**

| $\varepsilon_{Plastic}$ | 0.0 | 0.015 | 0.031 | 0.046 | 0.061 | 0.077 | 0.092 | 0.108 |
|---|---|---|---|---|---|---|---|---|
| $\sigma_{True}$ (N/mm$^3$) | 208 | 217 | 228 | 238 | 245 | 251 | 255 | 257 |

**Table 4  Material model for crushable foam (MAT_CRUSHABLE_FOAM)**

| Parameter | Description | Unit | Source |
|---|---|---|---|
| RO | Density | kg/mm$^3$ | Experiment |
| E | Young's modulus | GPa | Experiment |
| PR | Poisson's ratio | … | Experiment |
| LCID | Load curve ID for stress versus strain | … | Experiment |
| TSC | Tensile stress cutoff | GPa | Experiment |
| DAMP | Rate sensitivity via damping coefficient | … | Ref 51 |

**Table 5  Mechanical properties of foam**

| Material | RO | E | PR | TSC |
|---|---|---|---|---|
| Auxetic foam | $109 \times 10^{-9}$ | $4.23 \times 10^{-3}$ | $-0.31$ | $5.5 \times 10^{-4}$ |
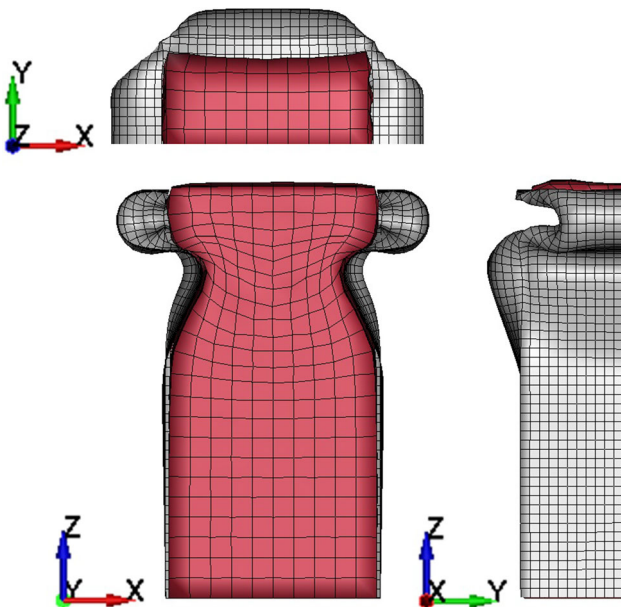


**Fig. 13** Orthogonal section views of FE model for foam-filled square tube

better understanding of the influence of wall thickness (*t*) on the deformation profile of auxetic foam-filled tube, a series of numerical simulations were carried out when the wall thickness varies from 0.4 to 1 mm. Other geometrical parameters such as tube diameter (*d*) and tube height (*h*) were kept constant.

Figure 16 indicates the deformation profiles of auxetic foam-filled circular tube at various wall thicknesses. From this figure, it appears that the number of created lobes for AFFCT significantly decreases as the tube wall thickness increases from 0.4 to 1 mm. It is noteworthy that the resistance of foam core to the tube wall intrusion gradually decreases as the wall thickness increases, which results in a reduction in the number of lobes. Moreover, the effect of wall thickness on the energy absorption-displacement response and the mean crushing force versus displacement response for AFFCT are presented in Fig. 17. From this figure, it is observed that increasing the wall thickness results in an increase in the EA and the MCF. The increase in the EA and MCF is attributed to the increased amount of material available for plastic buckling and subsequent EA and MCF (Fig. 17).

Although increasing the wall thickness enhances the energy absorption performance of the tube specimen in crushing process, a reduction in the number of created lobes is observed as the wall thickness increases. From energy absorption point of view, an increase in the number of created lobes increases the plastic deformation and subsequently interaction effect between foam core and tube walls. Hence, auxetic foam-filled tube with the wall thickness of 0.4 mm forms 8 lobes thereby seems to be more substantial than other wall thicknesses.

### 4.2 Influence of Tube Diameter on the Collapse Profile

The influence of tube diameter variations on the collapse profile of auxetic foam-filled circular tube was investigated using the validated FE model where the tube diameter varies from $d_0$ to $7/4 \, d_0$. Other geometrical parameters of circular tube such as wall thickness (*t*) and height (*h*) were kept constant.

Figure 18 illustrates the collapse profile of auxetic foam-filled circular tube at different tube diameters by keeping the crushing length constant at 48 mm. The results reveal that the deformation profile and progressive collapse of AFFCT are remarkably influenced by varying the tube diameter. In particular, two distinct patterns of collapse, namely concertina
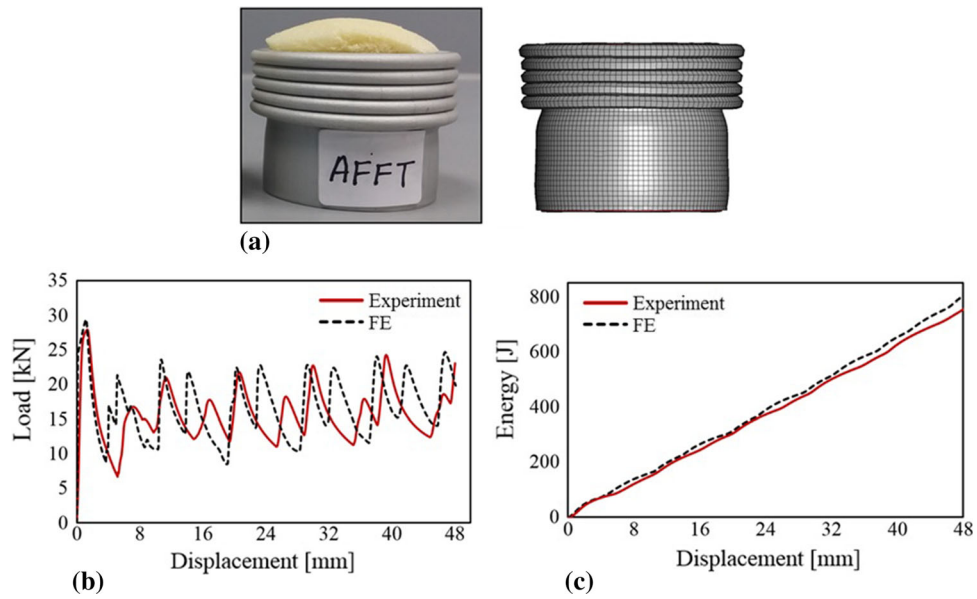
**Fig. 14** Comparison between experimental and numerical results for auxetic foam-filled circular tube; (a) collapse profiles, (b) load–displacement curves and (c) EA vs. displacement curves



**Fig. 15** Comparison between experimental and numerical results for auxetic foam-filled circular tube; (a) collapse profiles, (b) load–displacement curves and (c) EA vs. displacement curves
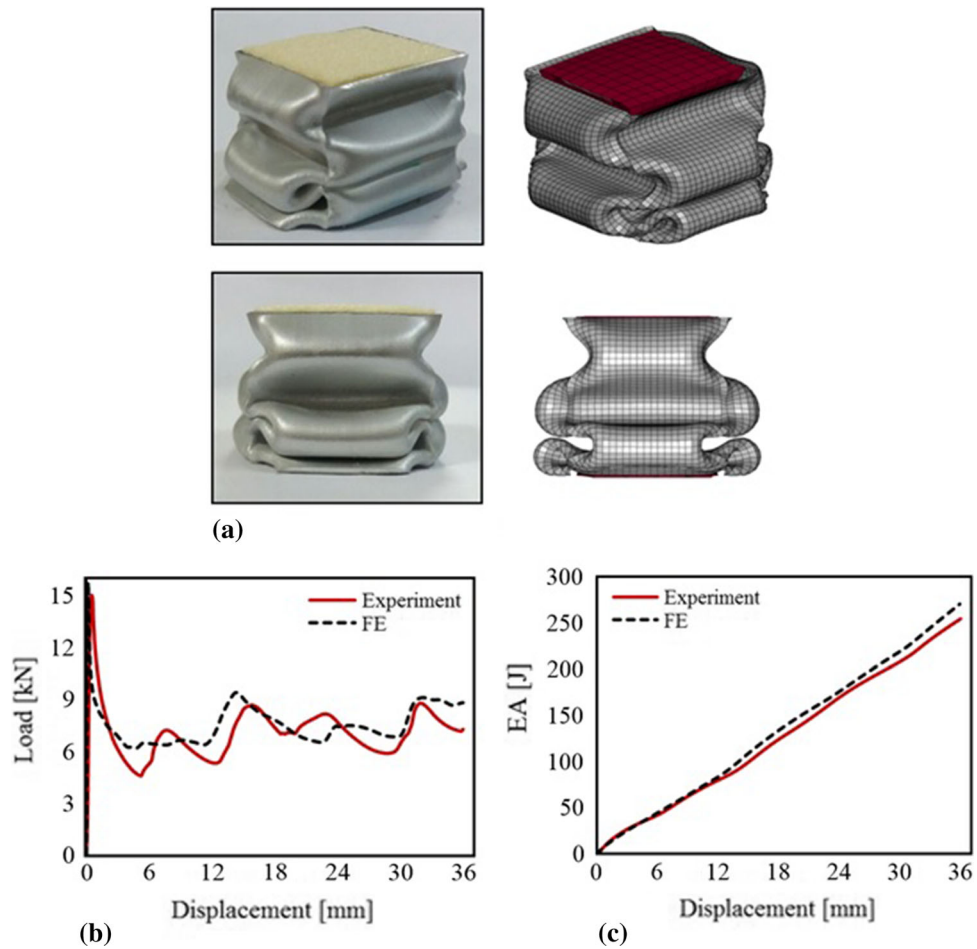
t = 0.4 mm — 8 Lobes
t = 0.6 mm — 7 Lobes
t = 0.8 mm — 6 Lobes
t = 1 mm — 5 Lobes

$d = d_0$, $h = h_0$; ($d_0 = 38$ mm, $h_0 = 80$ mm)
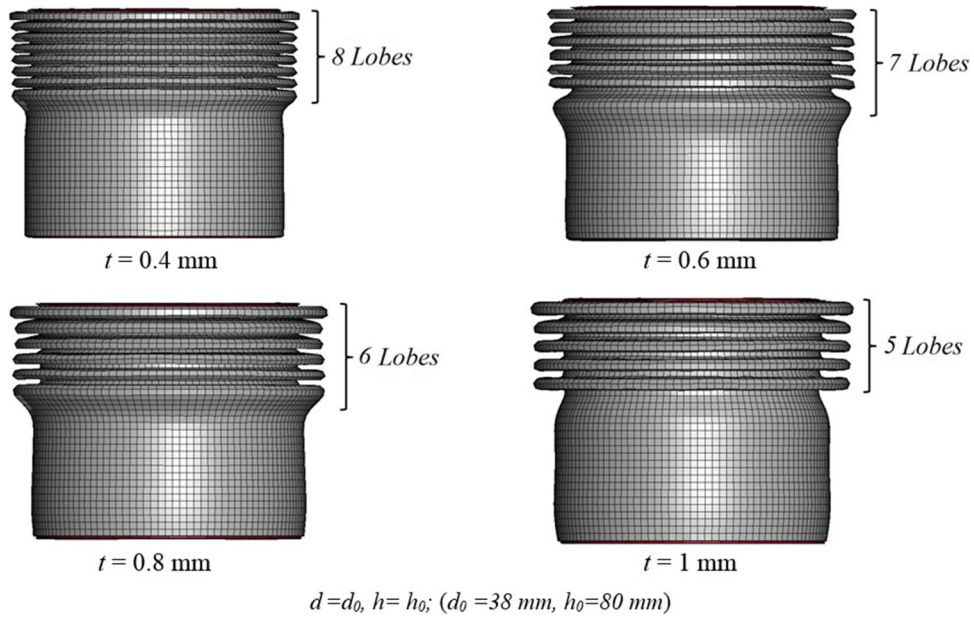
**Fig. 16** Influence of wall thickness on the collapse profile of AFFCT when the wall thickness varies from 0.4 to 1 mm



(a)

(b)
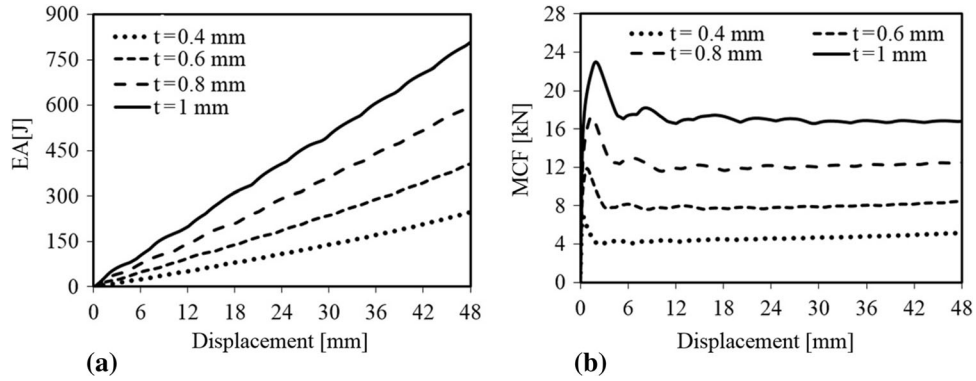
**Fig. 17** Influence of wall thickness on the (a) absorbed energy and (b) mean crushing force responses of AFFCT



$d = d_0$

$d = 5/4 \ d_0$

$d = 6/4 \ d_0$

$d = 7/4 \ d_0$

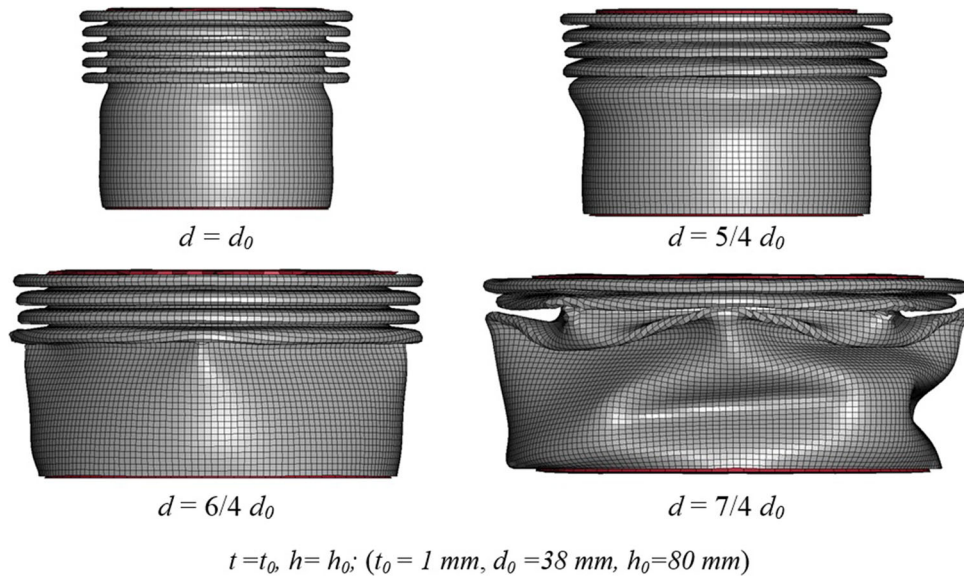$t = t_0$, $h = h_0$; ($t_0 = 1$ mm, $d_0 = 38$ mm, $h_0 = 80$ mm)

**Fig. 18** Influence of tube diameter on the collapse profile of AFFCT

pattern and diamond pattern are observed in the progressive buckling of AFFCT under quasi-static axial loading, as indicated in Fig. 18. From the detailed observation on the deformation profile of AFFCT, it is evident that the collapse profile shifts partially from the concertina profile to the diamond profile when the tube diameter is beyond $6/4d_0$, despite the presence of auxetic foam core. However, AFFCT collapse entirely in the concertina pattern (axisymmetric) when the tube diameter is less than $5/4d_0$. Nonetheless, the highest and the lowest crush stability were found for filled tubes with diameters of $d_0$ and $7/4\ d_0$, respectively.

From the discussion so far in the former section and this section, it can be seen that an increase in the tube diameter has a remarkable influence on the deformation mode of AFFCT (a considerable shift from the concertina mode to diamond mode occurred by increasing the tube diameter), while AFFCT tends to deform into a concertina mode as the wall thickness increases (Fig. 16). However, a reduction in the number of created lobes for AFFCT is observed when the wall thickness and tube diameter increase.

As the collapse mode of cylindrical tubes into concertina mode is more advantageous in energy absorbing systems than diamond and mixed modes, it can be concluded that the influence of tube diameter variations on the collapse mode of AFFCT is more substantial than wall thickness (Ref 57).

### 4.3 Influence of Wall Thickness on Energy Absorption Performance of AFFST

The influence of wall thickness on the response of auxetic foam-filled square tube is investigated in this subsection. Response parameters namely energy absorption, mean crushing force, initial peak load and crush force efficiency were analyzed in which all tube parameters are kept constant except wall thickness. In this case, the tube wall thickness was increased from 0.4 to 0.8 mm to allow meaningful comparison of results. Besides, loading condition and crushing distance were also kept constant. The tube dimensions are detailed in Table 6(a).

Figure 19 compares the influence of wall thickness variations on energy absorption (EA), mean crushing force (MCF), initial peak load ($P_{max}$) and crush force efficiency (CFE) for AFFST. It should be noted that all response parameters in Fig. 19 are demonstrated based on the wall thickness variations. From Fig. 19(a) and (b), it is observed that increasing the wall thickness results in an increase in the EA and the MCF. The increase in the EA is attributed to the increased amount of material available for plastic buckling and subsequent EA. Meanwhile, the effect of wall thickness on the MCF is quite similar to the mentioned response of EA, as the MCF is almost related to the energy absorbed as indicated in Fig. 19(b). It is also evident that in parallel with a slight increase in the wall thickness, initial peak load increases gradually as shown in Fig. 19(c). This is due to an increment in the amount of

material across the tube section, which effectively raises the axial stiffness of the tube and hence more crushing force is needed to commence plastic deformation. Overall, the dissipated energy, mean crushing force and initial peak load of filled tube is remarkably influenced by increasing tube wall thickness.

It can be clearly seen that increase in wall thickness is inversely proportional to crush force efficiency as demonstrated in Fig. 19(d). Nonetheless, the tube with 0.4 mm wall thickness still has the highest crush force efficiency. As aforementioned, by increasing the wall thickness, a significant increase in the MCF and Pmax can be achieved. Since increase in $P_{max}$ is more substantial and pronounced than enhancement of MCF and CFE is defined as the ratio of MCF to the Pmax, a slight reduction in the CFE is observed when the wall thickness is increases from 0.4 to 0.8 mm for both empty and foam-filled tubes. Overall, it can be concluded that increasing the wall thickness reduces the crush force efficiency response for a given height and width thus, use of thicker tubes is undesirable in crashworthiness design when CFE is considered as a design interest in energy absorbing devices. From Fig. 19(a), (b), (c), and (d), it is evident that the relationships between all crashworthiness indicators are almost linear. Therefore, the best linear curve fit with empirical formula was constructed for all crashworthiness indicators as shown in Fig. 19. These simple empirical formulae can be used to predict the quasi static axial crushing and energy absorption performance of auxetic foam-filled square tube for various thickness ($t$).

### 4.4 Influence of Tube Width on Energy Absorption Performance of AFFST

The influence of tube width variations on the crushing response of auxetic foam-filled square tube was examined using the FE model where the tube width varies from 0.75 $w_0$ to 1.75 $w_0$. Other geometrical parameters, viz., wall thickness and height, were kept constant. The geometrical parameters are given in Table 6(b). It is worth noting that all the presented results in this section were plotted based on dimensionless parameter, ratio of the tube width to height ($w/h$) where the height value is equal to $h_0$. The ratio of $w/h$ signifies slenderness ratio (SR).

The deformed profile for auxetic foam-filled square tube was compared at various widths by keeping the crushing length constant at 36 mm as shown in Fig. 20. It is evident that the progressive collapse and deformation mode of AFFST are pronouncedly affected by varying the tube width, so that the number of lobes created decreases as the tube width increases which could strongly influence the energy absorption performance of AFFST. From this detailed observation, it has been established that the number of collapse lobes, fold length and deformation mode are significantly influenced by the change in the tube width.

**Table 6 Dimensions of the models used in the FE analysis**

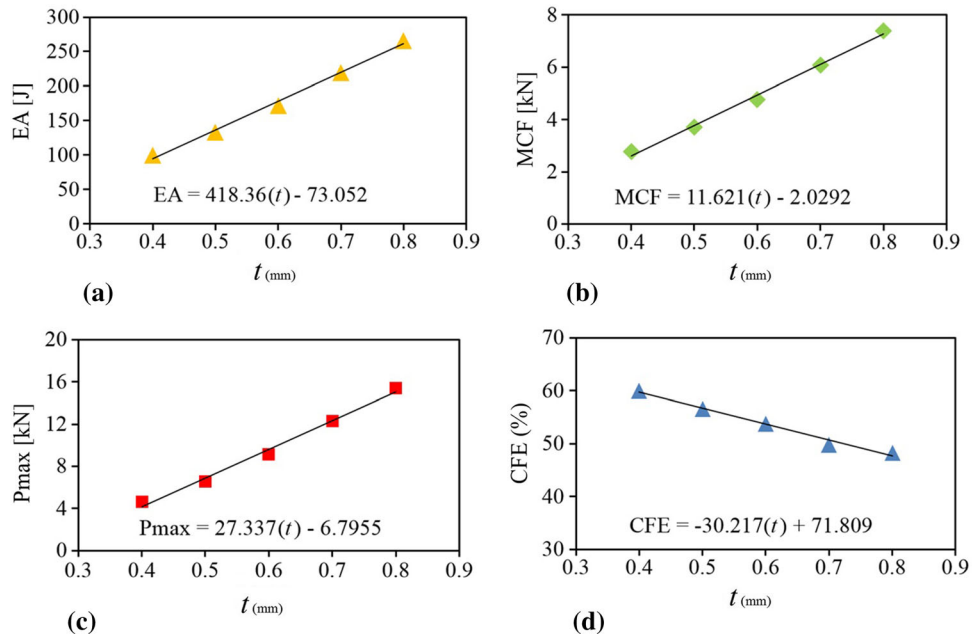| | a | | | b | | |
|---|---|---|---|---|---|---|
| Tube geometry | $w$ | $h$ | $t$ | $t$ | $h$ | $w$ |
| AFFST | $w_0$ | $h_0$ | 0.4, 0.5, 0.6, 0.7, 0.8 | $t_0$ | $h_0$ | $\frac{3}{4}w_0,\ w_0,\ \frac{5}{4}w_0,\ \frac{6}{4}w_0,\ \frac{7}{4}w_0$ |
| $w_0$ = 26 mm, $h_0$ = 60 mm, $t_0$ = 0.8 mm | | | | | | |

**Fig. 19** Influence of wall thickness on the crush response of AFFST: (a) EA, (b) MCF, (c) $P_{max}$ and (d) CFE
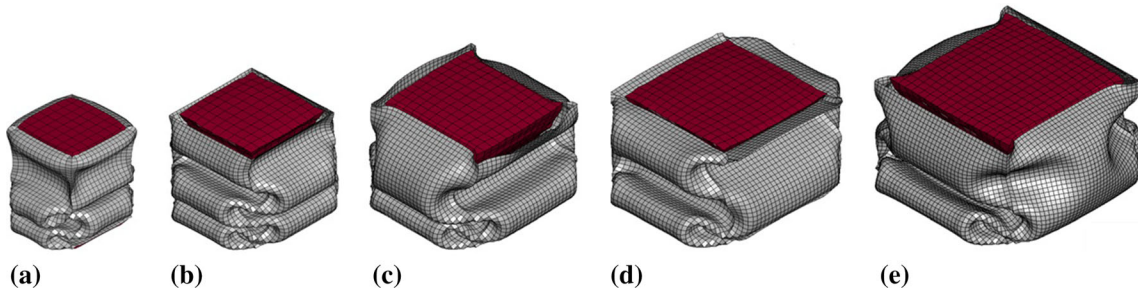


**Fig. 20** Deformation profiles for auxetic foam-filled tube where the tube width ($w$) is equal to (a) $0.75w_0$, (b) $w_0$, (c) $1.25w_0$, (d) $1.5w_0$ and (e) $1.75w_0$
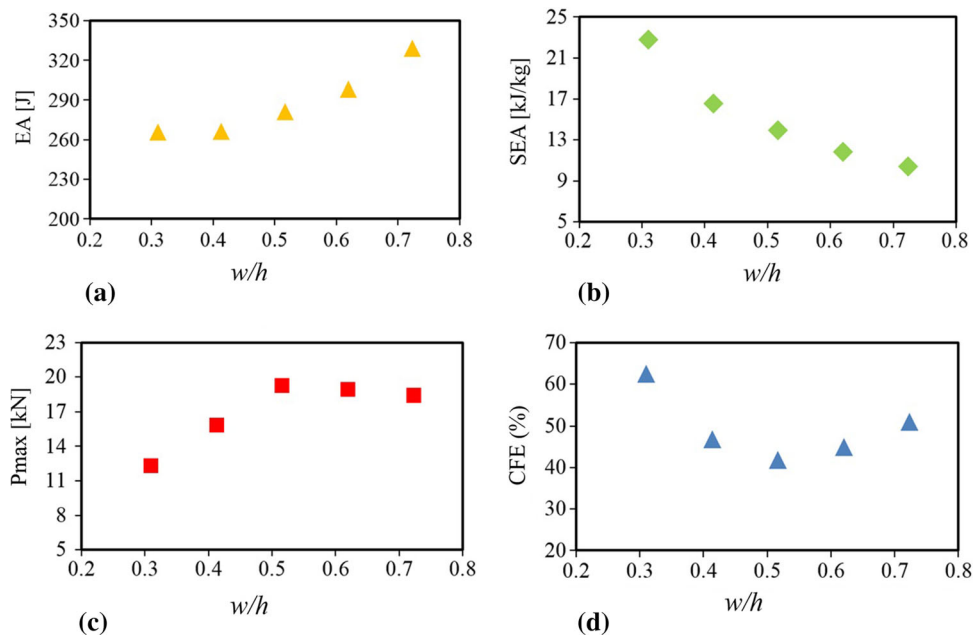


**Fig. 21** Influence of tube width variations on the crushing response of AFFT; (a) EA, (b) SEA, (c) $P_{max}$ (d) CFE

Figure 21 compares the influence of tube width variation on EA, specific energy absorption (SEA), $P_{max}$ and CFE responses for AFFST at constant crushing length of 36 mm. From this figure, it is obvious that the energy absorption of AFFST gradually increases with increase in $w/h$. The enhancement of the energy absorption response is indeed due to the involvement of more amount of auxetic foam material as the tube width increases, which provides extra absorbed energy during crushing. Based on the above finding, it is verified that the energy absorption shows more dependence on the tube wall thickness variations than on the tube width.

Figure 21(b) presents the influence of $w/h$ on the specific energy absorption for AFFST. It can be clearly seen that the SEA decreases as the tube width increases from 3/4 $w_0$ to 7/4 $w_0$. Nevertheless, AFFST with 19.5 mm tube width has the highest SEA than the other tubes. Overall, it appears that the SEA of AFFST is remarkably sensitive to $w/h$ variation. Conversely, $w/h$ variation for AFFST has insignificant effect on the EA.

Figure 21(c) demonstrates the influence of $SR$ on the initial peak load for auxetic foam-filled square tube. From this figure, it is evident that the initial peak load of AFFST gradually increases as $w/h$ increases from 0.32 to 0.54 but reduces beyond $w/h = 0.54$. Nonetheless, the lowest and highest initial peak load were presented by the tubes with the widths of 19.5 and 32.5 mm, respectively. An increase in the $P_{max}$ trend of AFFST up to $w/h$ of 0.54 is due to an increased amount of material available for plastic deformation as the tube width increases. Therefore, more crushing force is needed to initiate the buckling, leading to an increase in the initial peak load. Another possible reason could be related to a change in the stiffness of tube, the stiffness is defined as the structural property which is completely influenced by varying the geometrical parameters. As a matter of fact, the stiffness of tube to resist crushing load is increased as $w/h$ increases from 0.32 to 0.54 resulting in an increase in the initial peak Load. However, increasing $w/h$ of the tubes beyond 0.5 led to an increase in the amount of material available for crushing, but a decreasing trend is observed for AFFST. This is due to the reduction of tube's stiffness which is directly associated with the tube geometry. Overall, it can be concluded that the initial peak load of AFFST is less sensitive to SR beyond 0.54. In other words, the tube's stiffness was anticipated to continually decrease as SR increases beyond 0.54.

Figure 21(d) demonstrates the effect of $SR$ on the crush force efficiency of AFFST for a given height and wall thickness when the MCF is determined for crushing length of up to 36 mm. It is observed that the CFE initially decreases followed by a negligible increase. The trend shows that crush force efficiency is dependent on the variation of $w/h$. It should be mentioned that the variation in $w/h$ has less influence on the MCF for auxetic foam-filled square tube, hence, crush force efficiency can significantly be affected by varying the initial peak load. As shown in Fig. 21(d), CFE of AFFST dramatically decreases with increase in initial peak load at $w/h$ ranging from 0.32 to 0.54, but slightly increases as the $P_{max}$ decreases beyond $w/h$ of 0.54. Nevertheless, tubes with $w/h$ of 0.54 produce the highest and lowest initial peak load and crush force efficiency, respectively, which is undesirable in energy absorption applications.

## 5. Conclusion

This paper has numerically investigated the energy absorption performance of auxetic foam-filled square and circular tubes when loaded statically. Finite element computer simulations, validated by experimental results, were employed to obtain an insight into the axial crushing response, the deformation profile and the energy absorption capacity of square and circular tubes filled with polymeric auxetic foam for variations in the tube width ($w$), tube diameter ($d$) and wall thickness ($t$). The important remarks drawn from this present study are as follows.

a. Although, increasing the wall thickness enhances the energy absorption performance of AFFCT in crushing process, a reduction in the number of created lobes is observed as the wall thickness increases.
b. From the detailed observation on the deformation profile of AFFCT, it is evident that the collapse profile shifts partially from the concertina profile to the diamond profile when the tube diameter is beyond 6/4$d_0$.
c. It is evident that the progressive collapse and deformation mode of AFFST are pronouncedly affected by varying the tube width, so that the number of lobes created decreases as the tube width increases.
d. It is obvious that the energy absorption of AFFST gradually increases with increase in $w/h$, but SEA decreases as the tube width increases.
e. It is also noted that the initial peak load for AFFST is less sensitive to the tube slenderness ratio variations beyond $w/h = 0.54$.

## References

1. W. Abramowicz and N. Jones, Dynamic Axial Crushing of Square Tubes, *Int. J. Impact Eng.*, 1984, **2**(2), p 179–208
2. M. Langseth, O. Hopperstad, and A. Hanssen, Crash Behaviour of Thin-Walled Aluminium Members, *Thin-Walled Struct.*, 1998, **32**(1–3), p 127–150
3. S.P. Santosa, T. Wierzbicki, A.G. Hanssen, and M. Langseth, Experimental and Numerical Studies of Foam-Filled Sections, *Int. J. Impact Eng.*, 2000, **24**(5), p 509–534
4. Q. Wang, Z. Fan, H. Song, and L. Gui, Experimental and Numerical Analyses of the Axial Crushing Behaviour of Hat Sections Partially Filled with Aluminium Foam, *Int. J. Crashworthiness*, 2005, **10**(5), p 535–543
5. S. Mohsenizadeh, R. Alipour, Z. Ahmad, and A. Alias, Influence of Auxetic Foam in Quasi-static AXIAL Crushing, *Int. J. Mater. Res.*, 2016, **107**(10), p 916–924
6. S. Mohsenizadeh, R. Alipour, A.F. Nejad, M.S. Rad, and Z. Ahmad, Experimental Investigation on Energy Absorption of Auxetic Foam-

Filled Thin-Walled Square Tubes Under Quasi-static Loading, *Procedia Manuf.*, 2015, **2**, p 331–336

7. J. Bai, G. Meng, H. Wu, and W. Zuo, Bending Collapse of Dual Rectangle Thin-Walled Tubes for Conceptual Design, *Thin-Walled Struct.*, 2019, **135**, p 185–195

8. S. Reid, Plastic Deformation Mechanisms in Axially Compressed Metal Tubes Used as Impact Energy Absorbers, *Int. J. Mech. Sci.*, 1993, **35**(12), p 1035–1052

9. L. Aktay, A.K. Toksoy, and M. Güden, Quasi-static Axial Crushing of Extruded Polystyrene Foam-Filled Thin-Walled Aluminum Tubes: Experimental and Numerical Analysis, *Mater. Des.*, 2006, **27**(7), p 556–565

10. R.D. Hussein, D. Ruan, G. Lu, S. Guillow, and J.W. Yoon, Crushing Response of Square Aluminium Tubes Filled with Polyurethane Foam and Aluminium Honeycomb, *Thin-Walled Struct.*, 2017, **110**, p 140–154

11. R.D. Hussein, D. Ruan, G. Lu, and I. Sbarski, Axial Crushing Behaviour of Honeycomb-Filled Square Carbon Fibre Reinforced Plastic (CFRP) Tubes, *Compos. Struct.*, 2016, **140**, p 166–179

12. H. Yin, G. Wen, S. Hou, and K. Chen, Crushing Analysis and Multiobjective Crashworthiness Optimization of Honeycomb-Filled Single and Bitubular Polygonal Tubes, *Mater. Des.*, 2011, **32**(8–9), p 4449–4460

13. N. Gan, Y. Feng, H. Yin, G. Wen, D. Wang, and X. Huang, Quasi-static Axial Crushing Experiment Study of Foam-Filled CFRP and Aluminum Alloy Thin-Walled Structures, *Compos. Struct.*, 2016, **157**, p 303–319

14. J. Paz, J. Díaz, L. Romera, and M. Costas, Crushing Analysis and Multi-objective Crashworthiness Optimization of GFRP Honeycomb-Filled Energy Absorption Devices, *Finite Elem. Anal. Des.*, 2014, **91**, p 30–39

15. G. Balaji and K. Annamalai, Crushing Response of Square Aluminium Column Filled with Carbon Fibre Tubes and Aluminium Honeycomb, *Thin-Walled Struct.*, 2018, **132**, p 667–681

16. Z. Fan, G. Lu, and K. Liu, Quasi-static Axial Compression of Thin-Walled Tubes with Different Cross-Sectional Shapes, *Eng. Struct.*, 2013, **55**, p 80–89

17. A.A. Nia and M. Parsapour, Comparative Analysis of Energy Absorption Capacity of SIMPLE and Multi-cell Thin-Walled Tubes with Triangular, Square, Hexagonal and Octagonal Sections, *Thin-Walled Struct.*, 2014, **74**, p 155–165

18. W. Liu, Z. Lin, N. Wang, and X. Deng, Dynamic Performances of Thin-Walled Tubes with Star-Shaped Cross Section Under Axial Impact, *Thin-Walled Struct.*, 2016, **100**, p 25–37

19. Z. Fan, G. Lu, T. Yu, and K. Liu, Axial Crushing of Triangular Tubes, *Int. J. Appl. Mech.*, 2013, **5**(01), p 1350008

20. Q. Gao, L. Wang, Y. Wang, and C. Wang, Crushing Analysis and Multiobjective Crashworthiness Optimization of Foam-Filled Ellipse Tubes Under Oblique Impact Loading, *Thin-Walled Struct.*, 2016, **100**, p 105–112

21. G. Sun, S. Li, Q. Liu, G. Li, and Q. Li, Experimental Study on Crashworthiness of Empty/Aluminum Foam/Honeycomb-Filled CFRP Tubes, *Compos. Struct.*, 2016, **152**, p 969–993

22. C. Ge, Q. Gao, L. Wang, and Z. Hong, Theoretical Prediction and Numerical Analysis for Axial Crushing Behaviour of Elliptical Aluminium Foam-Filled Tube. *Thin-Walled Struct.*, 2019, **149**, p 106523

23. S. Shahbeyk, A. Vafai, and N. Petrinic, Axial Crushing of Metal Foam-Filled Square Columns: Foam Density Distribution and Impactor Inclination Effects, *Thin-Walled Struct.*, 2005, **43**(12), p 1818–1830

24. T. Reddy and S. Al-Hassani, Axial Crushing of Wood-Filled Square Metal Tubes, *Int. J. Mech. Sci.*, 1993, **35**(3-4), p 231–246

25. C. Gameiro and J. Cirne, Dynamic Axial Crushing of Short to Long Circular Aluminium Tubes with Agglomerate Cork Filler, *Int. J. Mech. Sci.*, 2007, **49**(9), p 1029–1037

26. A.G. Hanssen, M. Langseth, and O.S. Hopperstad, Static and Dynamic Crushing of Circular Aluminium Extrusions with Aluminium Foam Filler, *Int. J. Impact Eng.*, 2000, **24**(5), p 475–507

27. D. Tankara, R. Moradi, Y.Y. Tay, and H.M. Lankarani, Energy absorption characteristics of a thin-walled tube filled with carbon nano polyurethane foam and application in car bumper. In: ASME 2014 International Mechanical Engineering Congress and Exposition, American Society of Mechanical Engineers, 2014, p V012T15A029-V012T15A029

28. A.K. Toksoy and M. Güden, The Strengthening Effect of Polystyrene Foam Filling in Aluminum Thin-Walled Cylindrical Tubes, *Thin-Walled Struct.*, 2005, **43**(2), p 333–350

29. T. Reddy and R. Wall, Axial Compression of Foam-Filled Thin-Walled Circular Tubes, *Int. J. Impact Eng.*, 1988, **7**(2), p 151–166

30. T. Børvik, O.S. Hopperstad, A. Reyes, M. Langseth, G. Solomos, and T. Dyngeland, Empty and Foam-Filled Circular Aluminium Tubes Subjected to Axial and Oblique Quasistatic Loading, *Int. J. Crashworthiness*, 2003, **8**(5), p 481–494

31. L. Yan, N. Chouw, and K. Jayaraman, Effect of Triggering and Polyurethane Foam-Filler on Axial Crushing of Natural Flax/Epoxy Composite Tubes, *Mater. Des.*, 2014, **56**, p 528–541

32. M. Seitzberger, F.G. Rammerstorfer, R. Gradinger, H. Degischer, M. Blaimschein, and C. Walch, Experimental Studies on the Quasi-static Axial Crushing of Steel Columns Filled with Aluminium Foam, *Int. J. Solids Struct.*, 2000, **37**(30), p 4125–4147

33. G. Lu and T. Yu, *Energy Absorption of Structures and Materials*, Elsevier, Amsterdam, 2003

34. R. Lakes, Foam Structures with a Negative Poisson's Ratio, *Science*, 1987, **235**, p 1038–1041

35. F. Najarian, R. Alipour, M.S. Rad, A.F. Nejad, and A. Razavykia, Multi-objective Optimization of Converting Process of Auxetic Foam Using Three Different Statistical Methods, *Measurement*, 2018, **119**, p 108–116

36. Y. Prawoto, Seeing Auxetic Materials from the Mechanics Point of View: A Structural Review on the Negative Poisson's Ratio, *Comput. Mater. Sci.*, 2012, **58**, p 140–153

37. M. Bianchi, F.L. Scarpa, and C.W. Smith, Stiffness and Energy Dissipation in Polyurethane Auxetic Foams, *J. Mater. Sci.*, 2008, **43**(17), p 5851–5860

38. J. Choi and R. Lakes, Non-linear Properties of Polymer Cellular Materials with a Negative Poisson's Ratio, *J. Mater. Sci.*, 1992, **27**(17), p 4678–4684

39. R. Lakes, Design Considerations for Materials with Negative Poisson's Ratios, *J. Mech. Des.*, 1993, **115**(4), p 696–700

40. S. Hou, T. Liu, Z. Zhang, X. Han, and Q. Li, How Does Negative Poisson's Ratio of Foam Filler Affect Crashworthiness?, *Mater. Des.*, 2015, **82**, p 247–259

41. S. Mohsenizadeh, R. Alipour, M.S. Rad, A.F. Nejad, and Z. Ahmad, Crashworthiness Assessment of Auxetic Foam-Filled Tube Under Quasi-static Axial Loading, *Mater. Des.*, 2015, **88**, p 258–268

42. S. Mohsenizadeh and Z. Ahmad, Auxeticity Effect on Crushing Characteristics of Auxetic Foam-Filled Square Tubes Under Axial Loading, *Thin-Walled Struct.*, 2019, **145**, p 106379

43. A.A.S.f. Testing, Materials, *Standard Test Methods for Tension Testing of Metallic Materials*, ASTM International, West Conshohocken, 2009

44. S. Mohsenizadeh, Z. Ahmad, R. Alipour, R.A. Majid, and Y. Prawoto, Quasi Tri-axial Method for the Fabrication of Optimized Polyurethane Auxetic Foams, *Phys. Status Solidi (b)*, 2019, **256**(10), p 1800587

45. D. ASTM, 3574—Standard Test Methods for Flexible Cellular Materials—Slab, Bonded, and Molded Urethane Foams, 2001

46. J. Hallquist, *LS-DYNA Theoretical Manual*, Livermore Software Technology Corporation, Livermore, 2006

47. H.E. Boyer, *Atlas of Stress-Strain Curves*, Metals Park, ASM International, 1987, p 630

48. Z. Zhang, S. Liu, and Z. Tang, Comparisons of Honeycomb Sandwich and Foam-Filled Cylindrical Columns Under Axial Crushing Loads, *Thin-Walled Struct.*, 2011, **49**(9), p 1071–1079

49. Q.H. Shah and A. Topa, Modeling Large Deformation and Failure of Expanded Polystyrene Crushable Foam Using LS-DYNA, *Model. Simul. Eng.*, 2014, **2014**, p 1

50. D. Zangani, M. Robinson, and A. Gibson, Progressive Failure of Composite Hollow Sections with Foam-Filled Corrugated Sandwich Walls, *Appl. Compos. Mater.*, 2007, **14**(5–6), p 325–342

51. J.O. Hallquist, LS-DYNA® Keyword User's Manual Volume II Material Models, Livermore, California, USA, 2013

52. Z. Ahmad and D. Thambiratnam, Crushing Response of Foam-Filled Conical Tubes Under Quasi-static Axial Loading, *Mater. Des.*, 2009, **30**(7), p 2393–2403

53. V. Tarigopula, M. Langseth, O.S. Hopperstad, and A.H. Clausen, Axial Crushing of Thin-Walled High-Strength Steel Sections, *Int. J. Impact Eng.*, 2006, **32**(5), p 847–882

54. J. Reid and N. Hiser, Friction Modelling Between Solid Elements, *Int. J. Crashworthiness*, 2004, **9**(1), p 65–72

55. J.O. Hallquist, *LS-DYNA Keyword User's Manual*, Vol 970, Livermore Software Technology Corporation, Livermore, 2007, p 299–800

56. M. Barsotti, Comparison of FEM and SPH for Modeling a Crushable Foam Aircraft Arrestor Bed. *Aerosp. J.*, 2012, **2**, p 16–37

57. S. Guillow, G. Lu, and R. Grzebieta, Quasi-static Axial Compression of Thin-Walled Circular Aluminium Tubes, *Int. J. Mech. Sci.*, 2001, **43**(9), p 2103–2123